Summary: Crystallization, melting and annealing of nanoparticles of tetracontane were simulated via a Monte Carlo method on the second nearest neighbor diamond (2nnd) lattice by including short- and long-range interactions. Nanoparticles can be obtained from an equilibrated tetracontane melt by increasing three periodic lengths to values that are effectively infinite. Nanoparticles, which contain 155 chains of $C_{40}H_{82}$, have been produced. After a deep quench from 473 K to 298 K, the crystallization process was investigated by the evolution of the density profile, fraction of bonds in the *trans* state, and the orientational order parameter. The vicinity of the center is less dense and less well ordered than portions of the nanoparticle located further from the center. The crystals form first in the region close to the surface. Each nanoparticle usually contains multiple crystalline domains. A melting phenomenon was observed at a temperature about 365 K when the nanoparticle crystal was heated. Annealing of the multiple domain crystal at 360 K can transform the structure to a more regular one without a grain boundary.

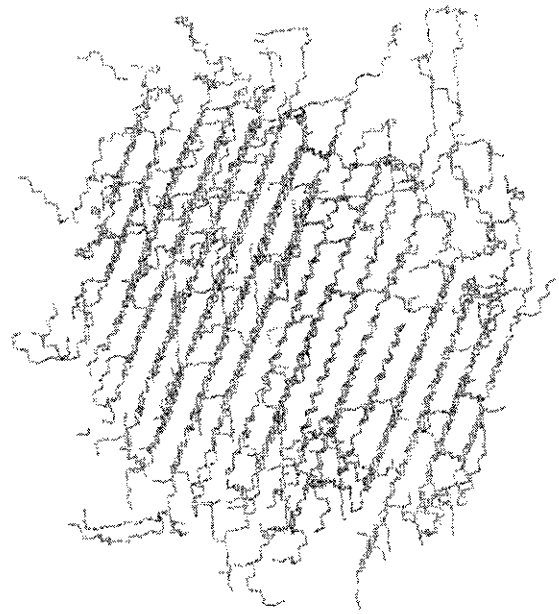

Snapshot of the final structure containing a single domain crystal after 20 million MCS.

Structure Formation in the Crystallization and Annealing of Tetracontane Nanoparticles

Visit Vao-Soongnern,[1] *Guoqiang Xu,*[2a] *Wayne L. Mattice*[2]

[1] School of Chemistry, Suranaree University of Technology, Nakhon Ratchasima, Thailand 30000
Fax: +11 66 44 224185; E-mail: visit@ccs.sut.ac.th
[2] Department of Polymer Science, The University of Akron, Akron, OH 44325-3909, USA

Received: December 12, 2003; Revised: April 20, 2004; Accepted: April 29, 2004; DOI: 10.1002/mats.200300048

Keywords: annealing; crystallization; Monte Carlo simulation; nanoparticles

Introduction

Structure formation of chain molecules is an interesting topic in chemistry, physics and biology, and has attracted the attention of many researchers. Since chain molecules have many internal degrees of freedom, structure formation proceeds in a complex fashion. Intensive experimental studies have been made on various structure formation processes of chain molecules. For example, the crystallization of polyethylene (PE) has been investigated by various time-resolved measurements.[1–3] Although considerable experimental investigations have been made, the detailed mechanism of structure formation on the molecular level is not completely understood.

It is well known that the surface structures of chain molecules play important roles in determining physical properties, such as adhesion and wetting. Therefore, studies of chain molecular systems with free surfaces are very important from the viewpoint both of chemical physics and of engineering. Recently, an experimental technique was developed for creating very fine polymer particles of arbitrary composition and size.[4–7] These particles in the

[a] Present address: Baker Laboratory of Chemistry and Chemical Biology, Cornell University, Ithaca, NY 14853-1301, USA.

 DOI: 10.1002/mats.200300048

nanometer size range provide many unique properties due to the size reduction to the point where critical length scales of physical phenomena become comparable to or larger than the size of the structure. Applications of such particles take the advantage of a high ratio of surface area to volume and the confinement effect, which leads to nanostructures with properties that differ from conventional materials. An example of the dependence of physical properties on size is the melting point for gold which, as is well known, decreases dramatically as the size decreases.[8] One of the major reasons for this phenomenon is the high ratio of surface area to volume and hence reduction of the non-bonded interactions for the surface layer. Clearly, such changes offer extraordinary potential for developing new materials in the form of bulk composites and blends that can be used for coatings, opto-electronic components, magnetic media, ceramics and special metals, micro-or nano-manufacturing, and bioengineering.[9,10]

The key to beneficially exploiting these interesting materials and technology is a detailed understanding of the connection of nanoparticle technology to atomic and molecular origins of the process. Computer simulation is one of the strongest tools for investigating the molecular mechanism of the structure formation for this system. While real free-standing nanoscale polymer melts may present difficulties in experimental studies in the laboratory, their models are easily created and studied in computer simulations.[11–25]

A variety of structural and physical characteristics of nanometer scale PE particles were studied by a large scale molecular dynamic (MD) simulation for a model generated with up to 120,000 atoms.[26–31] This simulation method creates homogenous nanoparticles that are in good agreement with 2-D diffraction observations on experimentally generated polymer nanoparticles. Structural characteristics, thermal and mechanical properties of these nanoparticles were reviewed in a recent publication.[7,10] Prior to these works, MD simulations of dynamics, conformational defects, plastic deformation, melting and reorganization of nanometer size crystals without constraints were performed for chain-like polymers.[32–38] It was found that a significant disorder existed at temperatures well below the melting point. As the temperature increases, the crystal of 192-$C_{50}H_{100}$-chains (pentacontalyene) breaks up into domains of different orientations with respect to the CH_2-chain zigzag planes. These domains are dynamic and change orientation and boundaries on a picosecond time scale. This occurs at a temperature that is still about 50 K below the experimental melting point of pentacontane ($T_m = 365$ K).[36] For the case of the structure formation upon cooling from the melt, a small particle of short chain molecules (100 chains of 20 CH_2 groups)[39,40] and the crystal growth of eicosane ($C_{20}H_{42}$) under a surface potential[41] have been investigated by MD simulations. In these works, the chains were initially equilibrated at high temperature and then the structure formation at a temperature below its melting point was monitored as a function of the simulation time. There was no grain boundary observed in the crystal obtained from these MD simulations.

We have previously performed Monte Carlo (MC) simulations of a short chain molecular system with (thin film[25] and nanofiber[42]) and without free surface (bulk[43]). It was found that the orientationally ordered structure is formed at low temperature by a sudden cooling from an amorphous configuration equilibrated at high temperature and the formation of the orientational order proceeds in a stepwise fashion. For the case of thin film simulations, the quick quench rapidly produces independently nucleated crystals with different orientations on each surface. The final structure retains a (less ordered) grain boundary in the middle of the films. In several independent simulations, one might sometimes get the single domain crystal without grain boundary if the two independently nucleated crystals happen to have the same orientation. Further simulations demonstrate that the imperfect structure, with grain boundary, spontaneously converts to the more perfect structure when it is annealed at the temperature about 10 K below the melting point.[25] The amorphous nanofiber was also studied in a similar manner as the thin film. A deep quench caused the nanofiber to produce a single crystalline domain, in which the chains are oriented parallel to the fiber axis. This is in contrast to the rapid crystallization found in the thin film. A less ordered, lower density region persists near the axis of the nanofiber. Removal of this defect by annealing is more difficult than removal of the grain boundary in the case of the thin film.[42]

In this work, we extend this investigation to the structure formation of a nanoparticle that is confined to free space, instead of the one or two surfaces that were present in the nanofiber[42] and thin film,[25] respectively. This work is also a continuation of the previous studies of the static and dynamic properties of an amorphous PE nanoparticle above the melting temperature by the same MC technique.[44]

Simulation Methodology

Model

The simulations are performed on a high coordination ($10i^2 + 2$ sites in shell i) lattice using coarse-grained chains.[45] The lattice can be constructed by eliminating every other site from a diamond lattice. If the C–C bond length is the step length on the precursor diamond lattice, the high coordination lattice has a step length of 0.25 nm. The angle between any two axes along the sides of the unit cell is 60°. Each occupied site contains a C_2H_4 or C_2H_5 unit of tetracontane, and each molecule is represented by a string of 20 such beads. The coarse-grained chains on this high coordination lattice can be reverse-mapped into a fully atomistic description, and the atomistically detailed chain

conformations in continuous space can be recovered after energy minimization.[46]

Energy

The Hamiltonian has two parts, one contribution from the short-range intramolecular interactions and the other contribution from all other interactions of the beads. The short-range intramolecular interactions are treated by the rotational isomeric state (RIS) model of Abe et al.,[47] which is mapped onto the coarse-grained chains using energies for the first- and second-order interactions of 2.1 and 8.4 kJ/mol.[48] The remaining interactions are represented by a discrete form of a continuous Lennard-Jones (LJ) potential energy function with $\varepsilon/k_B = 185$ K and $\sigma = 0.44$ nm. Discretization is obtained by a method which requires that the continuous and discretized LJ functions specify exactly the same value of the second virial coefficient for a nonideal gas.[49] The discrete shell energies used in the present simulations are the same ones as those tabulated in the description of the simulation of the thin film.[25]

Moves

Single bead moves are employed in the simulation with the restriction that a chain cannot pass through itself, as in a self-avoiding random walk. A randomly chosen bead can move to one of the vacant sites in its nearest neighbor shell if the attempt does not change the bond length to its bonded neighbors. Local bead moves on the 2nnd lattice are accepted according to the Metropolis algorithm.[50] The probability to move a bead within a chain is given by

$$P_{\text{move}} = \min[1, P_{\text{LR}} P_{\text{new}}/P_{\text{old}}] \quad (1)$$

Here, $P_{\text{LR}} = \exp(-\Delta E_{\text{LR}}/RT)$ is the probability from the change in the long-range interaction energy (ΔE_{LR}), and $P_{\text{new}}/P_{\text{old}}$ is the ratio of the probabilities for the new and old local conformations according to the short-range interaction. Dynamic MC simulations are performed after mapping the chains on this coarse-grained lattice. In the simulations, each Monte Carlo step (MCS) is equal to a series of single bead moves, in which all the beads in the system are randomly attempted once on average. The moves on the lattice correspond to the displacement of two or three backbone atoms on the real PE chain.

Nanoparticle Formation

The nanoparticle used in this simulation is initially constructed by the method described in our previous work.[44] First, bulk *NVT* simulations are performed at 473 K with 155 parent chains of 20 beads (tetracontane) each in a periodic box with a length of 24 lattice units on each side. This box imposes a density typical of a semi-crystalline PE. After equilibration of this system above the melting point, the periodic length of the simulation box in each direction, which will be referred to as x, y, and z, is increased to 96 lattice units. The image of each parent chain that is retained for the subsequent simulation is the one with the most beads lying within the first 24 steps along each axis. This procedure eliminates the interaction of the chains with their images: i.e. no periodic boundary conditions are effective in any direction. The system is equilibrated at 473 K for two million MCS with the new boundary conditions to obtain the nanoparticle in the melt. Then the temperature is instantaneously dropped to 298 K, and the simulation is continued at 298 K. At least 10 million MCS is needed to observe the structure formation. The final replica from the simulation at 298 K is used for the melting and annealing studies. The melting temperature of the nanoparticle of tetracontane is about 365 K (see the description in section *Transition Temperature*). For an annealing study, the temperature is instantaneously increased from 298 K to 360 K, which is about 5 K below the simulated melting temperature. Simulation of annealing is continued at this temperature.

Results and Discussion

Typical Crystallization of Nanoparticles at 298 K

Crystallization of the nanoparticle after instantaneously cooling from 473 K to 298 K, which is about 56 K below the experimental melting temperature of bulk tetracontane, is monitored using the density profile, fraction of the bonds in the *trans* state and the intermolecular orientation correlation function.

Structure Formation

Figure 1a and 1b illustrate a comparison between the configurations of 155 tetracontane chains at $T = 473$ K and $T = 298$ K (after a simulation of 30 million MCS). The snapshots have been reverse-mapped to restore all of the carbon atoms on the underlying diamond lattice. After cooling, the chains have a large amount of extended, planar zigzag conformations, and form regular domains with different orientation. Independent initiation of crystalline domains forces the formation of a less ordered domain, the so-called grain boundary, inside this nanoparticle. A single domain crystal has never been found from other several independent runs. A longer run up to 40 million MCS gave no noticeable change in the structure.

The intermolecular packing of chain molecules in the nanoparticle can be viewed as an intermediate structure between a uniform sphere and a cubic shape depending on the characteristics of packing. For example, if all chains orient perfectly parallel and form the all *trans* conformation, the final structure may be represented by a uniform rectangular box. In this work, the nanoparticle at 298 K

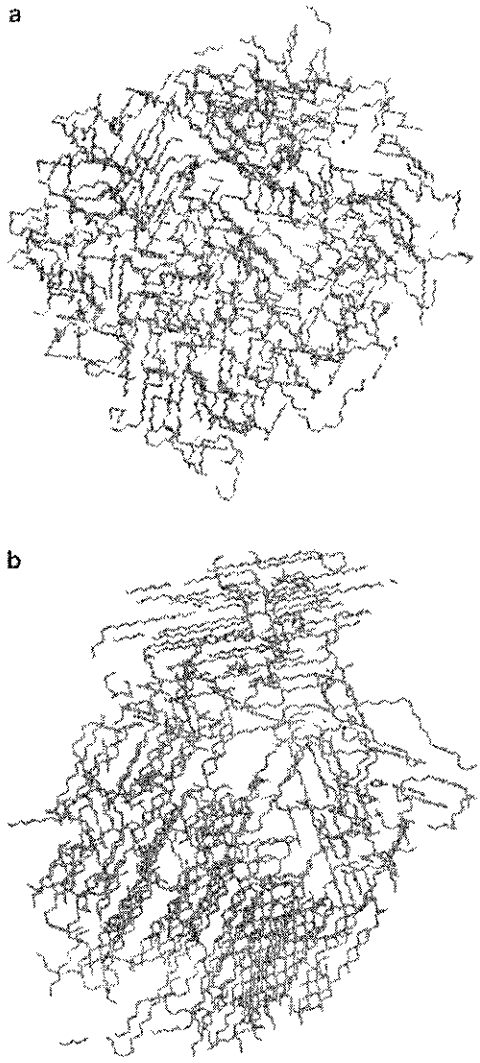

Figure 1. Snapshots of (a) the equilibrated nanoparticle structure at 473 K and (b) conformation of a typical nanoparticle at 298 K quenched from (a) at the end of 30 million MCS.

contains multiple crystalline domains with different orientations that cause the shape of the crystal different from the rectangular box. The result in Figure 1b suggests that the final structure may be more spherical in shape. In order to clarify this issue, the structure factor, $P(q)$, from the final snapshot at 298 K is calculated and compared with that predicted from the theoretical curve for a sphere. The structure factor from the simulation can be calculated by the following equation.

$$P(q) = \frac{1}{N_b^2} \sum_{i=1}^{N_b} \sum_{j=1}^{N_b} \frac{\sin(\boldsymbol{q} \cdot \boldsymbol{r}_{ij})}{q r_{ij}} \quad (2)$$

Here, N_b is the number of total beads in the snapshot; r_{ij} is the distance between two ethylene units; $\boldsymbol{q}$ is scattering vector with a length of $(4\pi/\lambda)\sin(\theta/2)$, where θ and λ are the scattering angle and the wavelength of incident beam, respectively.

Figure 2 shows the structure factor, $P(q)$, versus scattering vector, q, and the fitting of the uniform sphere model defined as

$$P(q)_{\text{sphere}} = 9(qR)^{-6}[\sin(qR) - qR\cos(qR)]^2 \quad (3)$$

Here, R is the radius of sphere. The fitting gives R about 3.15 nm, which is in the range of the approximated radius of the nanoparticle determined from the density profile in Figure 3. This result suggests that the structure obtained at 298 K can be approximated by a sphere model. Fitting to the scattering factor for a uniform sphere with the equilibrated nanoparticle at 473 K (not shown) gives a less satisfactory result, perhaps because the surface region is broader (larger ξ in Equation (4) in the next section) in the amorphous particle at 473 K than in the ordered particle at 298 K.

Density Profile

The density profile is calculated by counting the number of 2nnd beads (before reverse-mapping but after converting to the Cartesian coordinate system) that fall into spherical bins of 0.4 nm thickness beginning from the center of the nanoparticle. In this figure and similar figures showing properties of the nanoparticle as a function of r, the sampling error increases as r approaches zero. Data becomes less reliable as r falls below 1 nm. This problem affects about 30% of the range of r, but only about 3% ($0.3^3 \times 100\%$) of the volume of the nanoparticle. The evolution of the density profiles, $\rho(r)$, is depicted in Figure 3. The values at 0 MCS are obtained from an equilibrated structure at 473 K. The density profiles at 10^4 and 10^5 MCS are averaged over ten independent runs. At later times, the $\rho(r)$ are averaged over 100 configurations near the stated time. Initially, the plateau

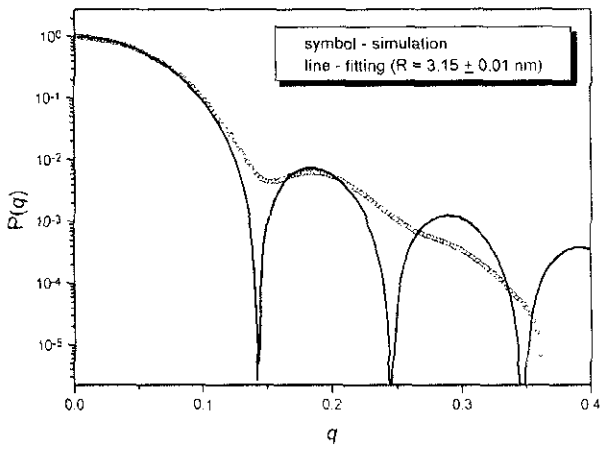

Figure 2. The structure factor, $P(q)$, versus scattering vector, q, of the crystalline nanoparticle (open circles) and the fitting from a uniform sphere model (solid curve).

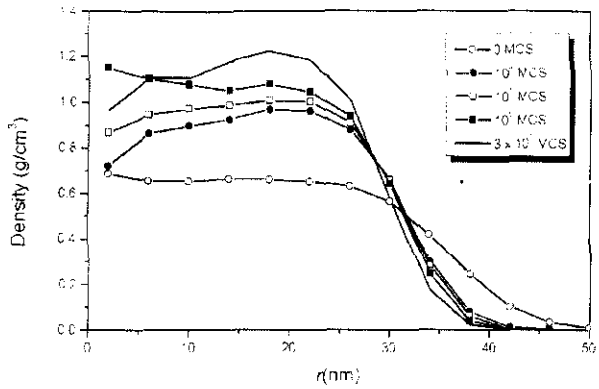

Figure 3. The evolution of the density profile, $\rho(r)$, as a function of MCS after an instantaneous cooling of the nanoparticle from 473 to 298 K.

bulk density, ρ_B, has a value in the range expected for an alkane melt, but it rapidly rises to a typical value of a crystalline PE. When $r < 1.0$ nm, the density fluctuates about an average value of approximately 1.15 g/cm^3, which could be regarded as the bulk density of the nanoparticle, ρ_B, in the simulation. This bulk density is affected by the choice of the LJ parameters, σ and ε, and by the number of shells used to calculate the long-range interactions. The present set of parameters gives a density within 15% of the experimental value for crystalline PE,[51] and is close to the bulk density obtained in the simulation of the thin film and nanofiber at the same temperature.[25,42] The densification of the interior of the nanoparticle is accompanied by a sharpening of the density profile in the surface region. The correlation length (ξ), obtained from the fit of the density profile in the surface region by the usual hyperbolic tangent function (Equation (4)), decreases by about a factor of two-third, from 0.65 to 0.46 nm, as the nanoparticle adapts to the lower temperature.

$$\rho(r) = \frac{\rho_B}{2}\left[1 - \tanh\left(\frac{r}{\xi}\right)\right] \quad (4)$$

The position for $\rho(r) = \rho_B/2$ is around 3.0 nm. The value of r at which $\rho(r) = \rho_B/2$ moves slightly closer to the center of mass of the particle during the simulation, as expected from the increase in the value of ρ_B. The density rises rapidly during the first 10^6 MCS. Prolongation of the simulation by an order of magnitude, to 10^7 MCS, produces no detectable change in the density very near the center of mass of the nanoparticle. The density for the portion of the nanoparticle in the region 1.5–2.5 nm increases more than other parts. This region is in accord with the location where the nucleation initiates.

Bond Conformation

In order to investigate the structure formation process on the molecular level, we first examine how the conformational change takes place. The RIS model for the unperturbed PE chain predicts that 58% and 64% of the bonds are in the *trans* state at 473 and 298 K, respectively.[52,53] Figure 4a depicts an evolution of the fraction of the bonds in *trans* states as a function of MCS after an instantaneous quench from 473 to 298 K. As the simulation of the nanoparticle proceeds, the chains adopt more *trans* conformation. After 25 million MCS, the fraction of the bonds in the *trans* states approaches a limiting value about 78%. This value is smaller than that of the crystallization in the bulk (ca. 85%) by the same MC method.[43] Therefore, chains adopt more *gauche* conformation for the crystallization in the nanoparticle. In Figure 4b, we plot the time dependence for the fraction of the bonds in the *trans* state versus the distance from the center of mass of the nanoparticle. The noise at very small r values is induced by the poor sample close to the center of the particle. The results show that chains are

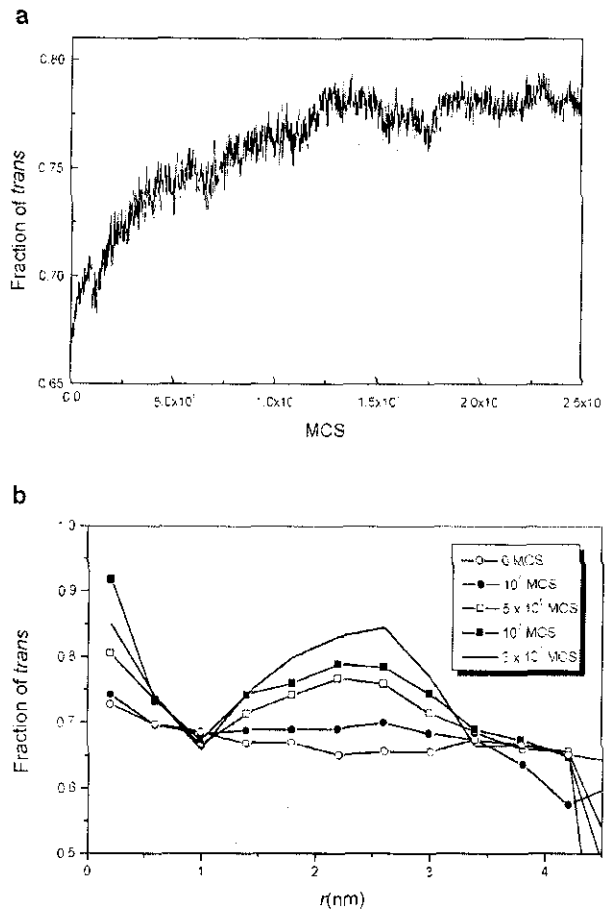

Figure 4. (a) Fraction of C–C bonds that are in the *trans* state as a function of MCS after an instantaneous cooling of nanoparticle from 473 to 298 K (b) Time dependence of the fraction of the bonds in the *trans* state versus the distance from the center of mass of the nanoparticle after an instantaneous cooling of the nanoparticle from 473 to 298 K.

gradually elongated in the region around 1.5–3.0 nm, which is in accord with the region of the crystalline domains. The density in this region is also larger than other portions as illustrated by the density profile at the late stage (10^7 MCS) in Figure 3. The change in the fraction of the bonds in the *trans* states for r less than 1.0 nm has a weaker correlation with the simulation time. This implies that the vicinity of the center is less dense and less well ordered than portions of the nanoparticle located further from the center. The orientation order parameter for the chord and end-to-end vector averaged in each bin also confirms this result (not shown). Here the orientation order parameters are calculated according to Equation (5) using the angles between two chord vectors or end-to-end vectors instead of Ψ.

Chain Ordering

A PE chain has zigzag *trans* conformation (torsion angle 180° at the internal C–C bonds) when it crystallizes. In a perfect crystalline domain, bonds have high correlation even at long distance. In order to investigate the growth process of an intermolecular orientational order, we calculate the global orientation correlation function, S_G, which is defined by Equation (5).

$$S_G = \frac{1}{2}\left[3\langle\cos^2\Psi\rangle - 1\right] \quad (5)$$

Here, Ψ denotes the angle between the main axes of two chains, and the value of S_G is averaged for all pairs of chains in a given snapshot. The main axis of a chain is the longest principal axis of the radius of gyration tensor. This parameter, S_G, has a value of 1.0 when all chains are parallel and that of 0.0 when all chains are randomly oriented. Figure 5 depicts the global orientation order parameter, S_G, as a function of MCS. S_G increases steadily at the beginning of the crystallization followed by an almost constant value in the late stage. The chains finally achieve $S_G \sim 0.15$ which is substantially smaller than the crystallization in the previous bulk simulation ($S_G \sim 0.8$).[143] This result suggests that chains in the nanoparticle are less ordered compared to the crystallization in the bulk or multiple domains form. By comparing Figure 5 with Figure 4a, it is concluded that the ordering of molecules correlates with the chain stretching. These results are slightly different from the previous simulation for the bulk system[140,143] in which the ordering of chains starts after the chains are stretched to a certain extent. The difference might be induced by the crystallization in different domains with various orientations in the present case.

We also investigated the time evolution of the orientational order parameter of the main axis of chains averaged from all pairs of molecules in each bin as a function of the distance from the center (Figure not shown). The result indicates that chains become more parallel in the region 1.5–2.5 nm. This finding and the results from Figure 3 and 4b confirm that nucleation starts in the surface region and then the crystals are formed independently when chains are elongated and aligned in parallel orientation.

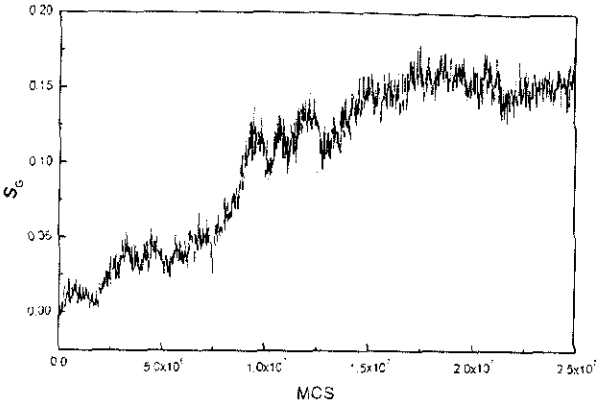

Figure 5. The global orientation order parameter, S_G, as a function of MCS after an instantaneous cooling of the nanoparticle from 473 to 298 K. The square radii of gyration of the chains (R_g^2) are 0.64 nm^2 and 0.79 nm^2 in the melt and in the crystal at 298 K (the last point in the figure), respectively.

Transition Temperature

Three parameters were used to investigate the transition temperature of the nanoparticle crystal obtained from the quick quench of the melt. They are the probability of *trans* conformation of C–C bonds, P_t, orientation order parameter of all coarse-grained bonds, S_b, and the orientation order parameter of the largest principal moment of the radius of gyration tensor of the chain, S_G (also called the global orientation order parameter). The definition of S_b is similar to the one for S_G in Equation (5), with the substitution of the angle between two coarse-grained bonds (ψ) for the angle between two major principal axes (Ψ).

$$S_b = \frac{1}{2}\left[3\langle\cos^2\psi\rangle - 1\right] \quad (6)$$

Simulations were performed at various temperatures, always starting from the typical structure (with multiple crystalline domains) obtained at 298 K. Figure 6 shows the temperature dependence of the limiting values of P_t, S_b and S_G. At low temperatures, they have large values due to a highly ordered crystalline structure, while at high temperatures they have much smaller values. The values change sharply near 365 K. Therefore, T_m of the nanoparticle determined by the parameters used in this simulation is around 365 K. (It should be noted that the large increase of the parameters at 360 K is induced by the annealing effect, which improves the regularity of the crystal of the nanoparticle.) This value is smaller than the T_m obtained in the previous simulation of a thin film (ca. 390 K) with the same set of parameters.[125] A reduction of T_m is caused by the larger surface/volume ratio in the case of the

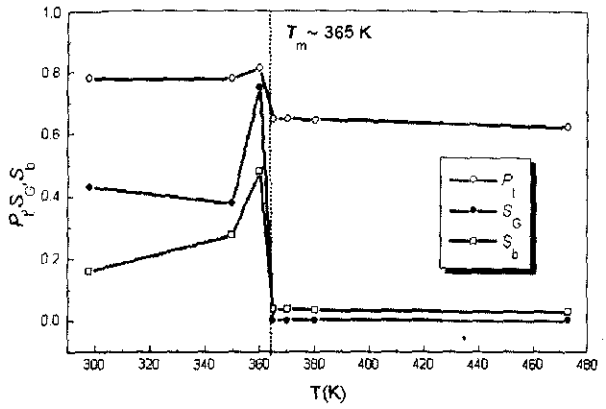

Figure 6. Temperature dependence of the limiting values of P_t, S_G, and S_b obtained at different temperatures.

nanoparticle. The final total energy, intermolecular and intramolecular energy at different temperatures also have a sharp increase around 365 K (not shown). The T_m obtained from the present simulations lies between the experimental T_m of the bulk tetracontane (354.5 K)[54] and that of bulk crystalline PE (414–419 K).[51] The surprising result that the experimental T_m of bulk tetracontane is about 10 K lower than the simulated T_m for the nanoparticle could be fixed by reducing slightly the size of ε in the LJ potential, as described earlier in the simulation of the melting of thin films.[25] Since the precise value of T_m is not of concern of the present study, that refinement in the LJ potential has not been made here.

The Melting Process

Figure 7 depicts the evolution of P_t, S_b and S_G when the structure at 298 K is instantaneously raised to 370 K. As the simulation proceeds at 370 K, all three parameters

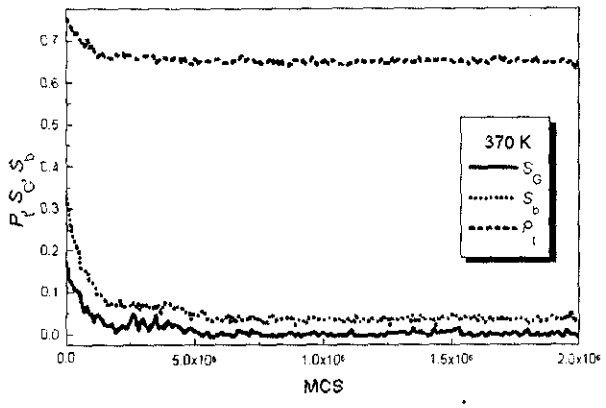

Figure 7. Fraction of the *trans* conformation of C–C bonds, P_t, orientation order parameter of all coarse-grained bonds, S_b, and global orientation order parameter, S_G, as a function of MCS in the melting process of the nanoparticle at 370 K. The initial configuration of the nanoparticle was a typical (multiple crystalline domains) one obtained at 298 K.

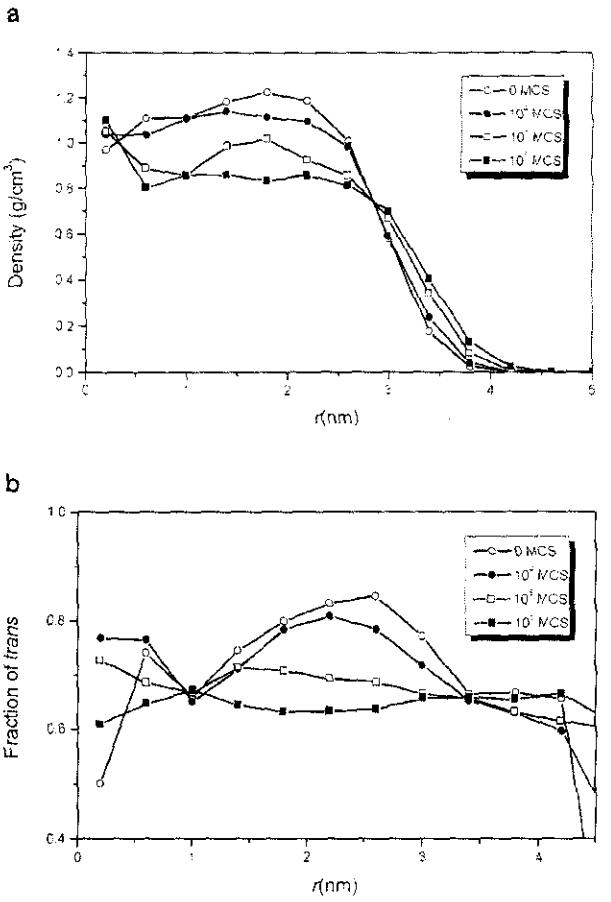

Figure 8. (a) The change in density profile of the nanoparticle when a typical (multiple crystalline domains) configuration at 298 K is instantaneously heated to 370 K (b) The change in fraction of the bonds in the *trans* state as a function of the distance from the center of mass upon a melting process of the nanoparticle. The initial configuration of the nanoparticle was a typical (multiple crystalline domains) one obtained at 298 K and was heated to 370 K.

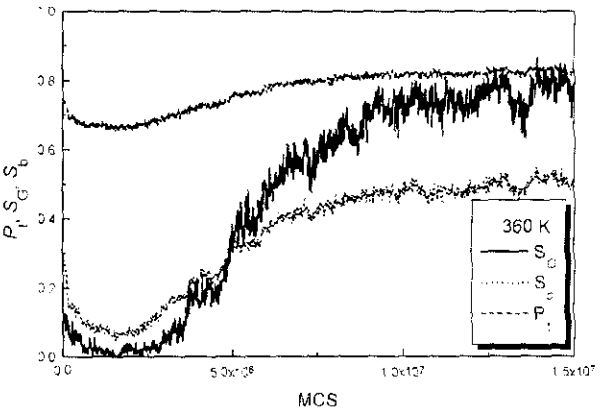

Figure 9. P_t, S_b, and S_G as a function of MCS in the annealing process of the nanoparticle at 360 K. The initial configuration of the nanoparticle was a typical (multiple crystalline domains) one obtained at 298 K.

Table 1. The limiting values of P_t, S_G, and S_b for different simulation conditions.

Parameter	298 K (crystallization)	360 K (annealing)	473 K (melting)
P_t	0.78	0.82	0.65
S_G	0.16	0.75	0.00
S_b	0.43	0.48	0.03

decrease from their values at 298 K and eventually reach new values at 370 K. For S_b and S_G, the final values are closed to zero, indicating the nanoparticle at 370 K has reached a state in which coarse-grained bond vectors and radius of gyration tensors are randomly oriented. The fraction of C–C bonds in the *trans* state falls from ca. 0.78 to a characteristic value of the melt (ca. 0.65).

Figure 8a shows the change in the density profile upon the melting process of the nanoparticle with multiple crystalline domains at 370 K. The bulk density reaches the new plateau within 10^6 MCS. The density of the crystalline region (1.5–2.5 nm) decreases while the interface becomes broader. In a similar manner, Figure 8b illustrates the time dependence of the fraction of the bonds in the *trans* states as a function of the distance from the center of mass of the nanoparticle. This result suggests the melting starts from the portion of the crystal close to the free surface as indicated by a faster reduction of the fraction of the bonds in the *trans* state and density at 2.5–3.0 nm than those at 1.5–2.0 nm. The evolution of the order parameters and snapshots showed that the crystal in the surface region melts first followed by the melting of the inner core of the particle. This result is similar as other computer simulations on

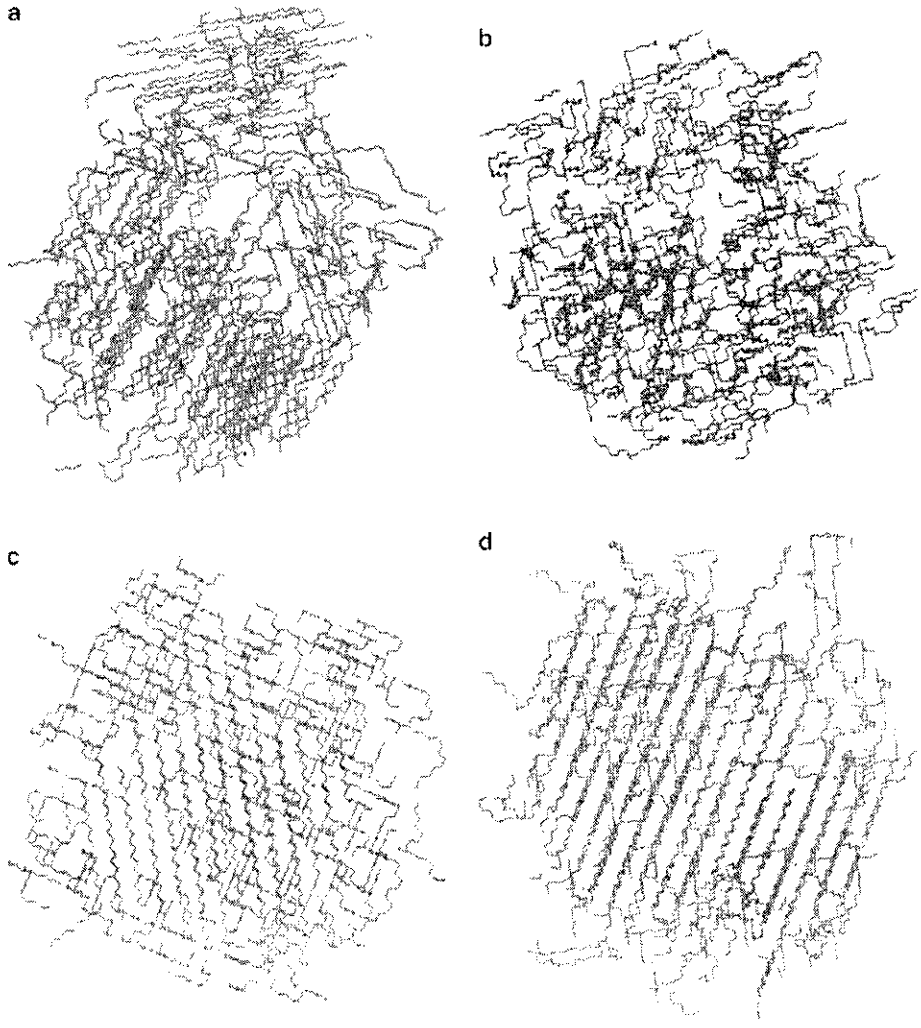

Figure 10. Snapshots of (a) the nanoparticle structure at 298 K, the structure for an annealing of the nanoparticle at 360 K (b) after 2 million MCS, (c) after 5 million MCS, and (d) the final structure containing a single domain crystal after 20 million MCS. (Different orientations of crystalline domains in (c) and (d) are induced by the different rotation during the plotting.)

the surface[25,39,40] and an evidence of a Lindermann type mechanism of melting.[55]

The Annealing Process

In this section, we heated the nanoparticle crystal (with multiple crystalline domains obtained at 298 K) to a temperature slightly below its melting point. Here, the temperature 360 K (about 5 K below the T_m obtained from the simulation) is chosen to follow the annealing process. Figure 9 shows the evolution of P_t, S_b, and S_G during this process. At the beginning, all three parameters have relatively large values of $P_t = 0.78$, $S_b = 0.43$, and $S_G = 0.16$. These parameters decrease rapidly in the initial part of the simulation. The initial decrease of S_b and S_G is so rapid that the starting values are not apparent on the MCS scale used in Figure 9. After the decrease with the first 2 million MCS, these three parameters increase again and reach new values, which are much larger than those at 298 K. Table 1 lists the limiting values of these three parameters. The values of P_t, S_b, and S_G at 298 K and 360 K suggest that the nanoparticle annealed at 360 K forms a more regular structure than the starting crystal at 298 K.

In order to provide more insight into the mechanism of annealing, a series of the nanoparticle snapshots at different MCS are illustrated in Figure 10. At the beginning, the starting structure contains multiple crystal domains with different orientations (Figure 10a, same as Figure 1b). Then the structure seems to melt down within the first 2 million MCS since chains are disordered and the conformations become more random (Figure 10b). This finding is consistent with the values of $S_G \sim 0$ and $S_b \sim 0$ shown in Figure 9. After 2 million MCS, grain boundaries disappear, and the nanoparticle has achieved a new configuration in which most of the chains still have different orientations. However, no crystalline domain can be identified at this stage. For the snapshot at 5 million MCS in Figure 10c, most of chains reorient to the same direction and chain conformations become more stretched. Only one crystalline domain is observed. After a long simulation (20 million MCS in Figure 10d), there is no significant change in the crystal structure except the chains having more *trans* conformations. Few *gauche* conformations still appear and are located on the surface.

Figure 11a shows the change in the density profile of the nanoparticle crystal with multiple domains at 360 K. The density of the crystalline region (1.5–2.5 nm) drops from ca. 1.2 g/cm^3 to ca. 1.0 g/cm^3 during the first one million MCS. A longer run up to 10^7 MCS causes all portions of the nanoparticle to reach a new higher density (ca. 1.3 g/cm^3). Although the density of a single domain crystal is higher, the interfacial profile gives no noticeable difference from that of the crystal at 298 K. Next, we further proceed to study the time dependence of the fraction of the bonds in the *trans* states as a function of the distance from the center of

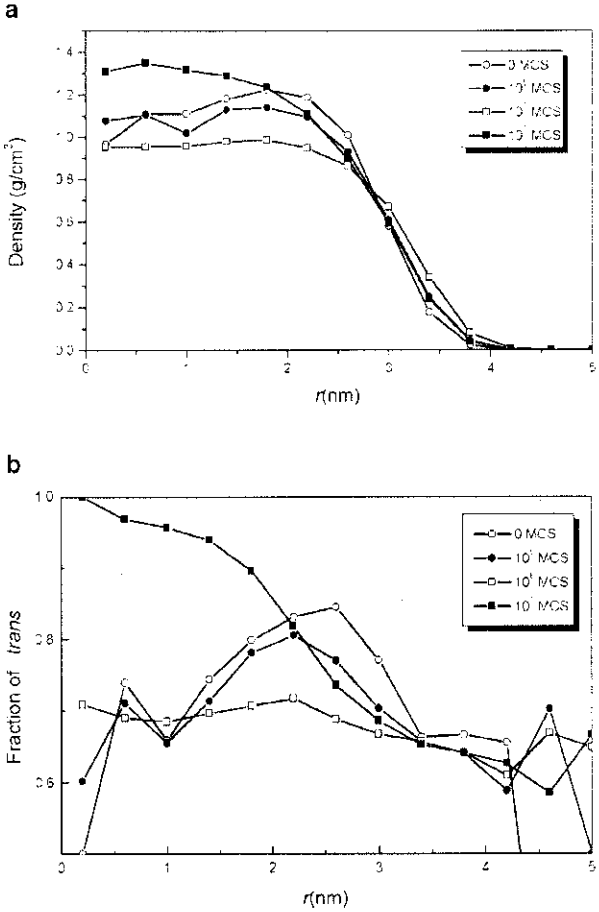

Figure 11. (a) The change in density profile and (b) the change in fraction of the bonds in the *trans* state as a function of the distance from the center of mass of the nanoparticle upon an annealing process at 360 K. The initial configuration of the nanoparticle was a typical (multiple crystalline domains) one obtained at 298 K and was heated to 360 K.

mass of the nanoparticle. Figure 11b suggests the mechanism of annealing in that the fraction of the bonds in the *trans* states in the crystalline domains near the surface decreases to ca. 0.65 within the first 10^6 MCS. P_t in the region $r = 2.0$–2.5 nm decreases faster than in the region $r = 1.5$–2.0 nm. For the simulation up to 10^7 MCS, we observe all *trans* conformation in the core region ($r = 0$–1.0 nm). The magnitude of P_t decreases monotonically toward the surface region. This result suggests that the crystal obtained after annealing is more ordered than the starting structure from a deep quench at 298 K. A longer run of this nanoparticle cannot transform this imperfect crystal to the perfect one ($P_t = 1.0$, $S_G = 1.0$, $S_b = 1.0$) in our simulation.

Conclusion

The crystallization of confined tetracontane ($C_{40}H_{82}$) quenched from the melt has been investigated by a dynamic

Monte Carlo method on a high coordination lattice. The periodic boundary conditions force the formation of a free-standing nanoparticle exposed to a vacuum. After a deep quench, the nanoparticle adopts a configuration dominated by extended chains. The vicinity of the center is less dense, and less well ordered, than portions of the nanoparticle located further from the center. The crystals are nucleated and formed in the surface region. A typical structure contains more than one crystalline domain. Chains in nanoparticle are less ordered and adopt more random conformation compared to the crystallization in the bulk.

The nanoparticle with multiple crystalline domains shows a well-defined melting temperature, around 365 K, obtained from a sharp decrease of P_t, S_G and S_h. The simulated result gives the melting point of nanoparticle lies between experimental T_m of bulk tetracontane and that of crystalline PE. The higher melting temperature obtained in the current simulation is induced by the strong attraction in the long-range interaction. However, this value is lower than that in the simulation of a thin film with the same set of parameters due to the high surface/volume ratio in the nanoparticle. A melting phenomenon was observed for any simulated temperature above 365 K when this nanoparticle was heated.

The annealing process finds that the nanoparticle with multiple crystalline domains can transform the imperfect crystal to a configuration with only one crystalline domain (without grain boundary). Annealing occurs when all crystalline domains become disordered, followed by the growth of a new crystalline region into the disordered region.

Acknowledgement: Financial supports from the *New Faculty Research Grant, Institute of Research and Development, Suranaree University of Technology, National Metal and Materials Technology Center (MTEC)* for Grant MT-S-43-POL-19-172-G (Thailand) are highly appreciated. GX and WLM thank the financial support from *National Science Foundation Grant* No. DMR 0098321 (USA).

[1] K. Tashiro, M. Izuchi, F. Kaneuchi, C. Jin, M. Kobayashi, R. S. Stein, *Macromolecules* **1994**, *27*, 1240.
[2] K. Tashiro, K. Imanishi, Y. Izumi, M. Kobayashi, K. Kobayashi, M. Satoh, R. S. Stein, *Macromolecules* **1995**, *28*, 8477.
[3] K. Tashiro, S. Sasaki, M. Kobayashi, *Macromolecules* **1996**, *29*, 7460.
[4] C. Y. Kung, M. Barnes, B. G. Sumpter, D. W. Noid, J. Otaigbe, *Polym. Prepr. (Am. Chem. Soc., Div. Polym. Chem.)* **1998**, *39*, 610.
[5] M. Barnes, K. C. Ng, K. Fukui, B. G. Sumpter, D. W. Noid, *Macromolecules* **1999**, *32*, 7183.
[6] US 6461546 (2002), invs.: D. W. Noid, J. U. Otaigbe, M. D. Barnes, B. G. Sumpter, C. Y. Kung.
[7] B. G. Sumpter, D. W. Noid, M. Barnes, *Polymer* **2003**, *44*, 4389.
[8] N. Ichinose, Y. Ozaki, S. Kashu, "*Superfine Particle Technology*", Springer-Verlag, London 1992.
[9] C. Hayashi, R. Uyeda, A. Tasaki, "*Ultra-Fine Particles Technology*", Noyes, New Jersey 1997.
[10] J. U. Otaigbe, M. D. Barnes, K. Fukui, B. G. Sumpter, D. W. Noid, *Adv. Polym. Sci.* **2001**, *154*, 1.
[11] W. G. Madden, *J. Chem. Phys.* **1987**, *87*, 1405.
[12] K. F. Mansfield, D. N. Theodorou, *Macromolecules* **1990**, *23*, 4430.
[13] K. F. Mansfield, D. N. Theodorou, *Macromolecules* **1991**, *24*, 6283.
[14] J. G. Harris, *J. Phys. Chem.* **1992**, *96*, 5077.
[15] S. K. Kumar, T. P. Russell, A. Hariharan, *Chem. Eng. Sci.* **1994**, *49*, 2899.
[16] O. F. Olaj, T. Petrik, G. Zifferer, *J. Chem. Soc., Faraday Trans.* **1995**, *91*, 2551.
[17] S. Misra, P. D. Fleming III, W. L. Mattice, *J. Comput.-Aided Mater. Des.* **1995**, *2*, 101.
[18] M. Ito, M. Matsumoto, M. Doi, *Fluid Phase Equilib.* **1998**, *144*, 395.
[19] P. Doruker, W. L. Mattice, *Macromolecules* **1998**, *31*, 1418.
[20] P. Doruker, W. L. Mattice, *Macromolecules* **1999**, *32*, 194.
[21] P. Doruker, W. L. Mattice, *J. Phys. Chem. B* **1999**, *103*, 178.
[22] M. Muller, L. G. MacDowell, *Macromolecules* **2000**, *33*, 3902.
[23] J. H. Jang, R. Ozisik, W. L. Mattice, *Macromolecules* **2000**, *33*, 7663.
[24] T. C. Clancy, J. H. Jang, A. Dhinojwala, W. L. Mattice, *J. Phys. Chem. B* **2001**, *105*, 11493.
[25] G. Xu, W. L. Mattice, *J. Chem. Phys.* **2002**, *116*, 2277.
[26] K. Fukui, B. G. Sumpter, M. Barnes, D. W. Noid, J. Otaigbe, *Polym. Prepr. (Am. Chem. Soc., Div. Polym. Chem.)* **1998**, *39*, 612.
[27] F. Fukui, B. G. Sumpter, M. D. Barnes, D. W. Noid, *Polym. J.* **1999**, *31*, 664.
[28] F. Fukui, B. G. Sumpter, M. D. Barnes, D. W. Noid, *Comput. Theor. Polym. Sci.* **1999**, *9*, 245.
[29] K. Fukui, B. G. Sumpter, M. D. Barnes, D. W. Noid, J. U. Otaigbe, *Macromol. Theory Simul.* **1999**, *8*, 38.
[30] K. Fukui, B. G. Sumpter, M. D. Barnes, D. W. Noid, *Macromolecules* **2000**, *33*, 5982.
[31] K. Fukui, B. G. Sumpter, D. W. Noid, C. Yang, R. E. Tuzun, *Comput. Theor. Polym. Sci.* **2001**, *11*, 191.
[32] G. L. Liang, D. W. Noid, B. G. Sumpter, B. Wunderlich, *Makromol. Chem., Theory Simul.* **1993**, *2*, 245.
[33] G. L. Liang, D. W. Noid, B. G. Sumpter, B. Wunderlich, *J. Polym. Sci., Part B: Polym. Phys.* **1993**, *31*, 1909.
[34] G. L. Liang, D. W. Noid, B. G. Sumpter, B. Wunderlich, *Comp. Polym. Sci.* **1993**, *3*, 101.
[35] G. L. Liang, D. W. Noid, B. G. Sumpter, B. Wunderlich, *Acta Polym.* **1993**, *44*, 219.
[36] B. G. Sumpter, D. W. Noid, G. L. Liang, B. Wunderlich, *Adv. Polym. Sci.* **1994**, *116*, 27.
[37] G. L. Liang, D. W. Noid, B. G. Sumpter, B. Wunderlich, *J. Phys. Chem.* **1994**, *98*, 11739.
[38] G. L. Liang, D. W. Noid, B. G. Sumpter, B. Wunderlich, *Polymer* **1995**, *36*, 109.
[39] S. Fujiwara, T. Sato, *Phys. Rev. Lett.* **1998**, *80*, 991.
[40] S. Fujiwara, T. Sato, *J. Chem. Phys.* **1999**, *110*, 9757.
[41] N. Waheed, M. S. Lavine, G. C. Rutledge, *J. Chem. Phys.* **2002**, *116*, 2301.
[42] G. Xu, V. Vao-Soongnern, W. L. Mattice, *Macromol. Theory Simul.* **2002**, *11*, 494.

[43] G. Xu, W. L. Mattice, *Comput. Theor. Polym. Sci.* **2001**, *11*, 405.
[44] V. Vao-Soongnern, R. Ozisik, W. L. Mattice, *Macromol. Theory Simul.* **2001**, *10*, 553.
[45] R. F. Rapold, W. L. Mattice, *J. Chem. Soc., Faraday Trans.* **1995**, *91*, 2435.
[46] P. Doruker, W. L. Mattice, *Macromolecules* **1997**, *30*, 5520.
[47] A. Abe, R. L. Jernigan, P. J. Flory, *J. Am. Chem. Soc.* **1966**, *88*, 631.
[48] R. F. Rapold, W. L. Mattice, *Macromolecules* **1996**, *29*, 2457.
[49] J. Cho, W. L. Mattice, *Macromolecules* **1997**, *30*, 637.
[50] N. Metropolis, A. W. Rosenbluth, M. N. Rosenbluth, A. H. Teller, E. Teller, *J. Chem. Phys.* **1953**, *21*, 1087.
[51] L. Mandelkern, R. G. Alamo, in: "*Polymer Data Handbook*", J. E. Mark, Eds., Oxford University Press, New York 1999, p. 501.
[52] P. J. Flory, "*Statistical Mechanics of Chain Molecules*", Wiley, New York 1969.
[53] W. L. Mattice, U. W. Suter, "*Conformational Theory of Large Molecules, The Rotational Isomeric State Model in Macromolecular Systems*", Wiley, New York 1994.
[54] L. Mandelkern, A. Prasad, R. G. Alamo, G. M. Stack, *Macromolecules* **1990**, *23*, 3696.
[55] F. A. Lindermann, Z. *Phys.* **1910**, *14*, 609.

